International Journal of Computing and Digital Systems
ISSN (2210-142X)
Int. J. Com. Dig. Sys. 16, No. 1 (Aug-24)

http://dx.doi.org/10.12785/ijcds/160177

Enhancing and Denoising Mammographic Images for Tumor Detection using Bivariate Shrinkage and Modified Morphological Transforms

Yen Thi Hoang Hua[1,3], Giang Hong Nguyen[1,3,4], Luong Bao Binh[2,3] and Dang Van Liet[1,3]

[1]*University of Science, Ho Chi Minh City, Vietnam*
[2]*Ho Chi Minh City University of Technology, Vietnam*
[3]*Vietnam National University Ho Chi Minh City, Vietnam*
[4]*Cao Thang Technical College, Ho Chi Minh City, Vietnam*

Received 25 Mar. 2024, Revised 17 May 2024, Accepted 17 May 2024, Published 16 Aug. 2024

Abstract: Breast cancer stands as a prevalent concern for women worldwide. Mammography serves as the frontline defense for early detection, yet its low X-ray dosage often leads to suboptimal image quality. This study proposes a multi-step solution: (i) Image enhancement employs a two-step approach: denoising using bivariate shrinkage and a hybrid median filter based on stationary wavelet transform (SWT) to avoid shift variants, and it is combined with modified morphology operations including the background, a vignette image with the weighting function $1/R^2$. (ii) Segmentation utilizes the fast K-means algorithm with a straightforward technique to select the number of clusters and tumors automatically, within the segment containing the largest centroid. (iii) Classification employs a boosting ensemble model, based on statistical features extracted from SWT coefficients at different levels, for tumor classification to achieve reliable results. Utilizing mammograms from the MIAS (Mammographic Image Analysis Society) public dataset, the proposed method was tested on Gaussian noisy images, demonstrating superior performance compared to existing algorithms in detecting lesions. The segmentation achieves a high accuracy, 98.15% on average and a specificity of 99.56%. However, the ground truth occasionally extends beyond the tumor mass, resulting in a low sensitivity of 62.81%. Finally, classification is also performed using boosting ensemble learning with accuracy of 100% for training, testing and real data.

Keywords: Breast Cancer, Mammogram, Stationary Wavelet Transform, Bivariate Shrinkage, Morphological Transform, Segmentation

1. Introduction

WHO (World Health Organization) data reveals 2.3 million breast cancer diagnoses and 685,000 deaths in 2020 [1]. Breast cancer casts a long shadow on global public health, impacting on numerous women and their families each year. The importance of early detection is widely recognized as a crucial element in improving patient outcomes and reducing mortality rates associated with breast, fibrous and glandular cancers.

An approach for early breast cancer detection is mammography, where specialized X-rays are used to scrutinize breast tissue. Yet, certain mammograms might be unclear and lack contrast, posing challenges in distinguishing tumors from dense breast tissue (comprising fibrous and glandular elements) due to their similar brightness levels. Therefore, noise reduction and contrast enhancement are essential preliminary measures before image analysis. Various denoising methods have been proposed, with wavelet denoising being widely used. Recent advancements in medical image processing, particularly denoising, enhancement, and detection techniques, are explored in this review.

Sendur et al. (2002) [2] presented an image denoising method based on discrete wavelets called bivariate shrinkage. When denoising with the nonlinear threshold, the new shrinkage functions determine the threshold for each coefficient based on the values of its parent and child within the wavelet decomposition, breaking away from the assumption of independence between wavelet coefficients. Therefore, the image denoising is better than the result achieved by the traditional method. Yin et al. (2011) [3] introduced a new image denoising method that models wavelet coefficients with a special distribution called the anisotropic bivariate Laplacian. This approach utilizes a corresponding shrinkage technique to remove noise, and for even better results, it was adapted to work within the DT-CWT domain. Fan et al. (2019) [4] presented a noise removal technique for images in the wavelet domain that utilizes wavelet thresholding and Wiener filtering. Benhassine et al. (2021) [5] proposed an

E-mail address: hthyen@hcmus.edu.vn, nguyenhonggiang@caothang.edu.vn, lbbinh@hcmut.edu.vn, dangvanliet@gmail.com

optimal image denoising method used for medical images using discrete wavelet transform (DWT). The obtained coefficients are thresholded using optimization algorithms. The performance of the method under different types of noise is determined by the criteria MSE (Mean Squared Error), PSNR (Peak Signal-to-Noise Ratio), and SSIM (Structural Similarity Index Measure).

Coffey et al. (2022) [6] explored the potential of Contrast-enhanced mammography (CEM) for breast cancer screening. CEM is a new imaging technique that combines traditional mammograms with contrast dye to show both structure and blood flow in the breast. It offers high accuracy in detecting breast cancer, especially in women with dense breasts, and is less expensive and more accessible than MRI scans. Tian et al. (2023) [7] proposed a method for denoising images using a multi-stage convolutional neural network that combines wavelet transformation and discriminative learning. Their method outperformed existing denoising methods in both quantitative and qualitative analysis.Liu et al. (2023) [8] addressed image denoising, a crucial step in image processing. They proposed a novel method based on wavelet transform and non-local moment mean filtering, achieving better denoising effects compared to other approaches.

J. Wu and C. Hicks (2021) [9] compared four machine learning methods, called Support Vector Machines (SVM), K-nearest neighbors (KNN), Naive Bayes, and Decision Trees, for mammogram classification. Their results demonstrated that SVM outperformed the other methods in terms of classification accuracy. Kittipol Wisaeng (2022) [10] employed a median filter to denoise mammograms and used the denoised images for tumor extraction applying Cuckoo Search to K-means clustering for the optimal cluster number selection. Razali et al. (2023) [11] address the challenge of dense breast tissue obscuring abnormalities in mammograms. They propose a textural-based enhancement technique. By analyzing breast density in each image, the technique tailors image processing to improve visibility of potential abnormalities. This targeted enhancement aims to benefit computer-aided diagnosis systems and potentially improve early cancer detection. Mourad Talbi and Riadh Baazaoui (2023) [12] employed soft thresholding on the detail components of the Stationary Wavelet Transform (SWT) for noise reduction. In addition to the noise reduction papers mentioned above, this section also reviews two recent studies on tumor detection and classification in mammograms, as they are relevant to the issues addressed by our proposed method.

The aforementioned studies demonstrated that noise reduction and contrast enhancement are performed separately. Noise reduction within the wavelet domain has traditionally treated components at different detail-component as independent, with the exception of the bivariate shrinkage method. In [2] and [3], the authors consider the correlation between parent and child wavelet coefficients of the Discrete Wavelet Transform (DWT). However, this approach has not been applied to the Stationary Wavelet Transform (SWT) and does not address contrast issues. In [9], machine classifiers are used individually, which necessitates a large number of instances to achieve satisfactory results. In [10], K-means is used for cluster selection, but the cluster containing the tumor requires a complex optimization search.

The contributions of the proposed approach aim to fill the gaps in the literature review:

(i) Utilizes wavelet-based image fusion for mammographic image enhancement. This enhancement method combines two techniques: denoising using stationary wavelet transform (SWT) with bivariate shrinkage, which considers the relationship between wavelet coefficients, and contrast enhancement using modified morphological operations.

(ii) Automatically selects clusters and identifies tumor-containing cluster for tumor detection using the fast K-means algorithm.

(iii) Extracts features from the enhanced image – instead of the segmented image – for ensemble learning-based tumor classification.

The rest of this paper is organized as follows. Section 2 reviews relevant theory, Section 3 details the proposed methodology, Section 4 presents the experimental results obtained, and Section 5 concludes the paper with future research directions.

2. Theoretical Background

A. Stationary Wavelet Transform

Wavelet analysis, valued for its time-frequency characteristics, finds significant use in image processing [13], particularly in denoising medical images like mammograms. Numerous research papers present this application [2-8]. The cornerstone of our denoising method is the use of the Stationary Wavelet Transform (SWT). The core functionality of SWT, similar to DWT, is image decomposition. It separates an image into four key components: approximation (A) capturing the overall structure, and detail components representing vertical (V), horizontal (H), and diagonal (D) features (Fig. 1) [14]. However, SWT performs upsampling of the coefficients of two low/high pass filters (Fig. 1a), so it maintains spatial localization and does not suffer from shift-variant problems. SWT handles edges and boundary effects more effectively than DWT, making it suitable for tasks such as image denoising and compression. As shown in Figure 1b, a single-level SWT decomposition of an MxN image produces four subbands: approximation(LL), horizontal detail (LH), vertical detail (HL), an diagonal detail (HH). These subbands have the same size MxN with the original image.

"À trous" is a common algorithm to calculate the Stationary Wavelet Transform (SWT) using a filter bank (h, g). The filters h are low-pass filters extracted from the scaling function, and the filters g are high-pass filters extracted from the wavelet function. For a 1-D signal, the algorithm produces a set of coefficients: w_j (high-pass filter) and c_j (low-pass filter) at scale j, given by:

$$c_j(k) = (\bar{h}^{j-1} * c_{j-1})[k] = \sum_l h[l] c_{j-1}[k + 2^{j-1} l] \quad (1)$$

$$w_j(k) = (\bar{g}^{j-1} * c_{j-1})[k] = \sum_l g[l] c_{j-1}[k + 2^{j-1} l] \quad (2)$$

where, $*$ denotes convolution and $h^j(k) = h(k)$ if $k/2^j$ is an interger and 0 for otherwise (Fig. 1a). So at each level, SWT coefficients have the same length as the original signal.

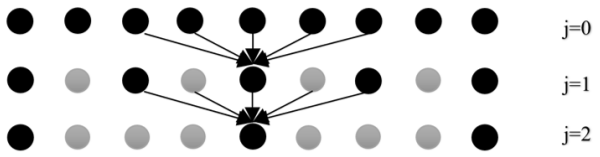

Black spot: filter coefficient; gray spot: zero padding
(a)

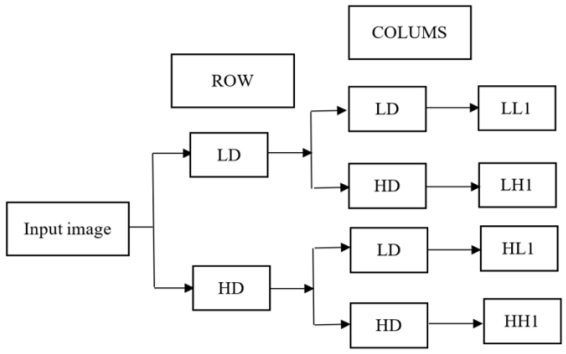

(b)

Figure 1. a) Padding 0 in the "À trous" filter, b) The flow-chart for single-scale SWT decomposition

As a result, c_0 (reconstruction) can be expanded as the sum of the wavelet coefficients $w_j(k)$ and the final smoothing data c_N:

$$c_0(k) = c_N + \sum_{j=1}^{N} w_j(k). \tag{3}$$

This algorithm can be extended to images (2-d signals): approximation coefficient:

$$c_j[k,l] = (\bar{h}^{j-1}\bar{h}^{j-1} * c_{j-1})[k,l], \tag{4}$$

detail coefficient in horizontal direction:

$$w_j^1[k,l] = (\bar{g}^{j-1}\bar{h}^{j-1} * c_{j-1})[k,l], \tag{5}$$

detail coefficient in vertical direction:

$$w_j^2[k,l] = (\bar{h}^{j-1}\bar{g}^{j-1} * c_{j-1})[k,l], \tag{6}$$

detail coefficient in diagonal direction:

$$w_j^3[k,l] = (\bar{g}^{j-1}\bar{g}^{j-1} * c_{j-1})[k,l] \tag{7}$$

where, $hg*c$ denotes convolution first along the rows and the convolution along the columns [15] (Fig. 1b).

B. Bivariate Shrinkage

Bivariate shrinkage for wavelet is an approach employed to diminish the presence of noise in images by utilizing the correlation between wavelet coefficients at different scales [16].

Consider an image degraded by Gaussian noise,

$$g = x + \varepsilon \tag{8}$$

where ε is Gaussian noise, g is observation image and x is an noise-free image. The problem for denoising is to find x from g by some criteria such that x is as close to the original image as possible.

Levent Sendur and Ivan W. Selesnick [2], modified

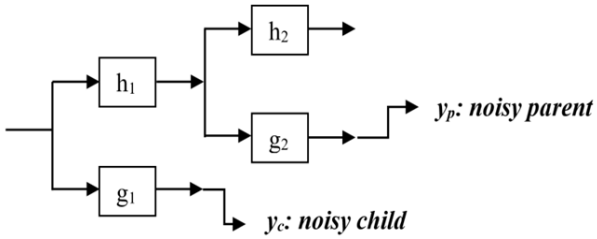

Figure 2. The analysis stage of bivariate shrinkage for wavelet decomposition

Bayesian estimation problem in the wavelet domain, has statistical dependence of the adjacent wavelet coefficients:

$$y = f + n \tag{9}$$

where, $\mathbf{y}(y_1, y_2)$, $\mathbf{f}(f_1, f_2)$, $\mathbf{n}(n_1, n_2)$ are respectively the wavelet coefficients of noisy image, free-noise image and noise; y_1 is the detail component of level k (child) and y_2 is the detail component of level $k+1$ (parent); these are two adjacent wavelet coefficients (Fig. 2).

According to Levent Sendur and Ivan W. Selesnick [2], the non-Gaussian bivariate probability density function given by:

$$P_{\mathbf{f}}(\mathbf{f}) = \frac{3}{2\pi\sigma^2} exp(-\frac{\sqrt{3}}{\sigma}\sqrt{f_1^2 + f_2^2}). \tag{10}$$

In this function, f_1 and f_2 are uncorrelated but not independent, with σ is marginal variance.

The MAP estimator of $\hat{f}_1$ produces the bivariate shrinkage function:

$$\hat{f}_1 = \frac{\sqrt{y_1^2 + y_2^2} - \frac{\sqrt{3}\sigma_n^2}{\sigma}}{\sqrt{y_1^2 + y_2^2}} . y_1. \tag{11}$$

The result shows that the estimated value of f_1, depends not only on y_1 (child wavelet coefficient) but also on y_2 (parent wavelet coefficient), showing that the formula has a parent-child dependency; so, the accuracy will be better than soft thresholding.

C. Dual Morphological enhancement

Image enhancement involves improving the contrast of an image, often through denoising techniques like histogram stretching or equalization. The most common method is histogram equalization, which rearranges the histogram to increase contrast. However, when the resulting image is used to detect tumors, the tumor locations are different from the ground truth tumor locations. Therefore, in order to avoid the above disadvantages, this article uses morphological operations with top-hat and bottom-hat transforms. The top-hat transform is obtained by subtracting the opened image from the original using a specific structural element, yielding an image that encompasses objects that are smaller than the structural elements and brighter for their surroundings. Conversely, the bottom-hat transform is derived from the disparity between the input image and its closing, generating an image highlighting objects that are smaller than the structuring elements and darker for their surroundings. Consequently, combining the denoised image with the top-hat filtered image and

then the bottom-hat filtered image is subtracted to obtain the contrast-enhanced image, which is called dual morphological enhancement [17].
- Top-hat transform:

$$T_{top-hat}(I) = I - (I \circ SE) \tag{12}$$

- Bottom-hat transform:

$$B_{bottom-hat}(I) = (I \bullet SE) - I \tag{13}$$

- Dual morphological enhancement:

$$I_{output} = I + T_{top-hat}(I) - B_{bottom-hat}(I) \tag{14}$$

where, I represents the original image, SE denotes the structuring element, $\circ$ the morphological opening operation and $\bullet$ the morphological closing operation.

D. K-means and Fast k-means

K-means is an unsupervised clustering algorithm that divides data into K different groups. In mathematical terms, the K-means algorithm aims to minimize the objective function:

$$J = \sum_{i=1}^{m} \sum_{k=1}^{K} w_{ik} \|x^i - \mu_k\|^2 \tag{15}$$

where, $w_{ik} = 1$ for the data point x_i if it belongs to cluster k, otherwise, $w_{ik} = 0$; μ_k represents the centroid of cluster k [18], [19].
The well-known K-means clustering algorithm suffers from a slow convergence rate. This limitation has motivated the development of faster variants, such as the fast K-means algorithm [20], [21]. According to Raied Salman et al. [21], the convergence rate is improved by dividing the distance calculation phase into two steps. Step 1, involves a fast distance calculation on a small subset data to determine the initial centroids. Step 2, calculates the exact distance over the entire data set using the initial centroids obtained in Step 1 to refine the centroids. The running time of this step is also minimized due to the lower number of iterations. Consequently, fast K-means converge quickly.

3. Proposed Methodology

The subsequent sections elaborate on these details.

A. Image Enhancement

One of the goals of this article is image enhancement, which involves removing noise and improving contrast. Therefore, only markers, artifacts and pectoral muscle are eliminated in the preprocessing stage. To avoid performing numerous operations that later lead to positioning errors of the detected tumor, these components are removed manually using Matlab software.

1) Denoising technique

Noise is a major factor affecting mammography. Therefore, denoising is required before segmenting the tumor. Fig. 3 shows the block diagram of the proposed denoising step for mammography images. In this proposed method, noise reduction in the wavelet domain is performed using a stationary wavelet transform. After decomposition, the detailed coefficients are denoised

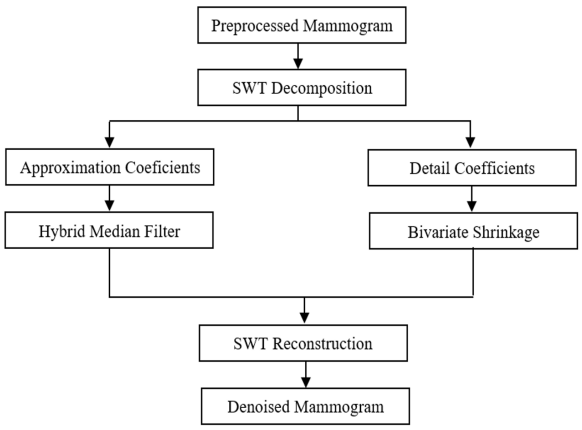

Figure 3. The block diagram for the proposed denoising methodology

using the bivariate shrinkage method, which removes noise but preserves features, as described in Section 2-B, and the approximate components are smoothed using hybrid median filtering. Denoised images in the spatial domain are obtained using the inverse stationary wavelet transform. This article uses the four wavelet functions bior2.2, db4, sym2 and coeif2 to find the optimal wavelet function for noise reduction.

2) Contrast enhancement

Mammograms have low tumor-to-background contrast. Therefore, contrast enhancement using dual morphological enhancement (Section 2-C) is required. In this article, formula (14) is modified by applying a high-pass filter, which sharpens the edges more effectively than using the original image. The high-pass filtered image is created by removing the background from the original image. The background image is typically obtained using average or low-pass Gaussian filtering. Here the background is a vignette image with a $1/R^2$ function, creating a bright center that fades toward the edges (vignette effect). This weighting function is multiplied by the original image to create the final background [22].

3) Fusion to image enhancement

Wavelet fusion combines two denoising and contrast enhancing images to create a fused image that retains the most relevant features and information from the original data.

B. Tumor Detection

In our proposed method, fast K-means is used for tumor detection. The number of clusters corresponding to the number of main peaks of the image histogram was automatically selected by a program that detects these peaks. In cluster analysis, the cluster containing the tumor corresponds to the cluster with the maximum centroid value. In this cluster, extract 3 to 5 images, each image contains a tumor (counted from the largest tumor), and select the image as the segment containing the tumor. The source code for fast K-means is given by Ankit Dixit [23].

C. Tumor Classification

Breast tumor classification aims to determine whether an image containing a mass is benign or malignant. In this

article, the classification typically involves a three-step process: pre-processing, feature extraction, and classification. The pre-processing stage focuses on enhancing image quality through techniques like denoising and contrast enhancement, as examined in Sections 3-A1 and 3-A2. This section introduces the steps of feature extraction and tumor classification.

1) Feature extraction

Feature extraction is a transformative process that aimes to condense the input data to reduce complexity and highlight salient features and attributes facilitating effective classification. This is a crucial step in classification and is performed directly on the input image to extract low-level features or on transformed images to capture high-level features. There are various methods for feature extraction; this article uses some statistical features to measure central tendency and data dispersion, which are listed in Section 4-D [24].

The above statistical features are extracted from the approximation and detail coefficients of SWT with different levels to obtain high-level features. The frequency bands of the approximation and detail coefficients in SWT vary from wide to narrow, corresponding to the levels from low to high. Therefore, the statistical features applied to the approximation and detail coefficients of SWT with different levels result in features at narrow and broad scales that captures sufficient properties of input classes for high classification accuracy. Statistical SWT features are contained in a feature matrix where the number of rows represents the instances and the number of columns represents the features.

2) Classifier design

This article employs ensemble learning, a diversification approach in machine learning that combines multiple classifiers – referred to as base classifiers or weak classifiers – such as decision trees and Naive Bayes, to construct a robust classifier. When the base classifiers are identical and trained in parallel, it's called a "bagging ensemble." In contrast, when the base classifiers are trained sequentially, it's called a "boosting ensemble" (which aims) to minimize errors in the training data. Boosting ensemble models are trained iteratively, where each subsequent model is trained on the misclassified predictions of the previous model. This results in a lower bias compared to individual base models. The final prediction is obtained by combining the weighted predictions of each base classifier. This approach not only achieves high accuracy but also exhibits faster computation time compared to bagging ensembles. Consequently, a boosting ensemble is employed in this article. The model is depicted in Figure 4.

The boosting ensemble model can be written as:

$$s_N(.) = \sum_{j=1}^{N} c_j w_j(.) \tag{16}$$

where, N is the number of weak models, c_j are the coefficients, and w_j are the weak models. To find the best model, Equation 16 is solved using an iterative approach:

$$s_j(.) = s_{j-1}(.) + c_j w_j(.) \tag{17}$$

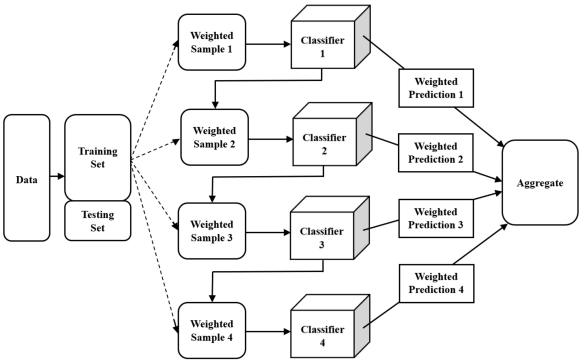

Figure 4. Boosting Ensemble Learning (Source: shiksha.com [25])

In the boosting ensemble method, the subsequent model (s_j) improves upon the previous model by selecting the class label (c_I) and weak learner (w_I) that are most consistent with the training data. The best model is then obtained as:

$$(c_j, w_j(.)) = \underset{c, w(.)}{argmin} E_r(s_{j-1}(.) + c_j w_j(.)) \tag{18}$$

where, $Er(.)$ represents the fitting error of the given model [26], [27].

Boosting ensemble encompasses two primary methods: Adaptive Boosting (AdaBoost) and Gradient Boosting [27]. Furthermore, Equation 16 has also been extended to develop Linear Programming Boosting (LPBoost) and Totally Corrective Boost (TotalBoost) [28].

4. Experimental Results and Discussion

A. Data and Equipment

The mammography images used in this study were provided by the well-known MIAS database [29]. This database contains 322 digitized mammograms at 50 micron resolution in "Portable Gray Map" (PGM) format of three types: normal (207), benign (63), and malignant (52). Each mammogram includes information about ground truth, its size and breast tissue structure. A mammography image (mdb001) was selected from the database for this study to investigate the optimization of noise reduction parameters. Ten images listed in Section 4-C were used for tumor detection, and one hundred images were used for classification.

The calculations for the proposed approach in Section 3 were implemented in the Matlab environment. All experiments were conducted on a laptop equipped with an AMD Ryzen 5 5600H processor, clocked at 3.30 GHz, and 8.00 GB of RAM.

B. Determine parameters for image enhancement

1) Determine the optimal parameters for noise reduction

In this article, we will only investigate Gaussian noise reduction because this type of noise is consistenly present in images. The examined image is mdb001 (Fig. 5a), which has been corrupted by Gaussian noise and has a mean of 0 and $\sigma = 25$ (Fig. 5b). After pectoral muscle removal, the image undergoes bivariate shrinkage noise reduction through the use of a stationary wavelet transform, selecting wavelet functions from three different wavelet families, namely biorthogonal wavelet functions

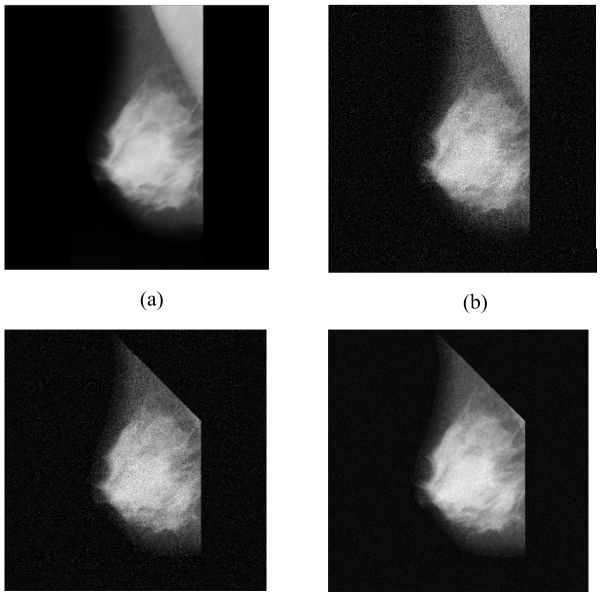

(a) (b) (c) (d)

Figure 5. a) Original mammogram mdb001, b) Noisy mammogram with Gaussian noise (σ = 25), c) Preprocessed mammogram, d) Denoised and contrast enhancement mammogram using the proposed method.

TABLE I. PSNR values of the proposed denoising method with Gaussian noise σ = 25

Wavelet	bior2.2	db4	sym2	coif2
SWT level 1	26.38	27.29	**27.36**	27.28
SWT level 2	25.40	27.15	27.05	27.08
SWT level 3	25.30	27.34	27.22	27.27
SWT level 4	25.29	27.36	27.19	27.31

(bior2.2), orthogonal wavelet functions with asymmetric (db4), orthogonal wavelet functions with asymmetry with different length (sym2 (length 2N) and coif2 (length 6N)). Noise reduction results are evaluated using the PSNR metric:

$$PSNR = 10log_{10}(\frac{MAX^2}{MSE}) \tag{19}$$

where, MAX is the maximum possible pixel value (255 for an 8-bit image) and MSE is the Mean Squared Error, which is calculated as the average of the squared differences between the processed image and the original.

Table I shows the experimental results of image denoising for the Gaussian noisy image mdb001 ($\mu = 0, \sigma = 25$) by PSNR of four wavelet functions (bior2.2, db4, sym2 and coif2) at the first to fourth levels of SWT.

According to the results presented in Table I, the proposed denoising method using bivariate shrinkage with SWT produces the best results when the sym2 wavelet function at level 1 or db4 at level 4 is used for comparison to other wavelet functions and the remaining levels. The Symlet family, a modification of the Daubechies family, exhibits near-symmetry in the complex linear phase and demonstrates remarkable effectiveness in noise reduction [30]. Additionally, Sym2 features a short-length filter, enabling rapid computation. Therefore, Sym2 at level 1 was chosen for noise reduction; along with level 1 decomposition, reveals that Gaussian noise with σ = 25 occupies approximately half of the high-frequency band of the image.

TABLE II. PSNR value of the proposed contrast enhancement method for mammogram contaminated with Gaussian noise σ = 25

Shape/Size	5	10	15	20
Disk	29.99	**30.04**	29.99	29.98
Square	29.99	30.02	29.97	29.99
Diamond	29.97	30.02	29.99	30.00

TABLE III. PSNR value of the proposed denoising method with different σ Gaussian noise.

σ	Mean-Mean	Max-Min	Max-Max
5	**42.49**	41.46	39.28
10	**37.06**	36.02	33.63
15	**33.62**	32.60	30.10
20	**31.16**	30.13	27.62
25	**29.65**	28.25	25.75
30	**27.75**	26.68	24.19

2) Determine the optimal structuring element for contrast enhancement

After wavelet-based bivariate shrinkage for noise reduction, the study of contrast enhancement is carried out by using modified top-hat and bottom-hat transforms with multiple sets of structuring element shapes such as disk, square, diamond with radii in the range of 5, 10, 15, 20 are utilized [31].

Table II presents the experimental results of contrast enhancement for the mammogram mdb001 contaminated with Gaussian noisy ($\mu = 0, \sigma = 25$) by PSNR for three shapes of structuring elements: disk, square, diamond with different size: 5, 10, 15, 20.

According to the results of Table II, structural elements with size 10 exhibit the highest PSNR values, which are relatively consistent across different shapes.

However, the symmetrical flat structural element is the most commonly used because it can be adapted to any object shape in the image. Therefore, a disk-shaped structuring element with a size of 10 is chosen for contrast enhancement.

3) Image for noise reduction and contrast enhancement

As described above, denoising using stationary wavelet-based bivariate shrinkage with sym2 wavelet function at the first level and the contrast enhancement using modified morphological operations with the disk shape in size 10 of structural elements achieves the best outcome. Therefore, to achieve both denoising and improved contrast, these two results are fused together using wavelet based image fusion techniques, for three cases mean-mean, max-min and max-max are performed. The results are presented in the Table III.

With varying standard deviation of Gaussian noise, the Mean-Mean method yields the optimal results as chosen in this article (Fig. 5d).

4) Compare the denoising results with other outcomes

In order to validate the above comment, the results are benchmarked against other thresholding algorithms in the article of [5] such as VisuShrink, Feed-forward denoising convolutional neural networks (DnCNN) and Benhassine et al. method [5] on the mdb001 mammogram with Gaussian noise using different standard deviations of 5, 10, 20 and 30, respectively. The results are shown in Table IV.

The value of PSNR for our proposed method is higher than all other enhancement techniques indicating better quality.

C. Tumor detection

The mammography enhancement (denoising and contrast enhancement) is then subjected to breast tumor detection using the fast K-means method. In this method, the breast tumor located in the segment with the maximum centroid value is extracted and smoothed using morphological operations.

In these experimental results, ten mammograms from the mini-MIAS database, representing five types of abnormality, are selected with two images for each category, because each type of abnormalities may have different characteristics. In the mini-MIAS database, each image provides ground truth for tumors. It is not represented in the actual shape but as a circle (with center and radius). Therefore, we ovelay the extracted breast tumor with a black circle representing the ground truth (provided by MIAS) on the original image to visualize the accuracy. To calculate the accuracy of the extracted tumor in comparison to the ground truth, the proposed method's extracted tumor is analyzed using the 'regionprops' function in Matlab to obtain its center coordinates, perimeter, area, and major and minor axes. The radius is calculated as the average of the major and minor axes of the tumor and the extracted circle which is represented by the white shaded area in the mammogram.

Circular (CIRC) mdb001 and mdb028, often appear as a well-circumscribed mass with uniform density throughout the lesion. The segmentation results, shown in Figures 6 and 7, indicate that the segmentation achieves good sensitivity. Miscellaneous (MISC) mdb063 and mdb058, exhibit significant variations in shape, edges, and internal density, which complicates diagnosis. Figures 8 and 9 illustrate the segmentation results. While the results for image mdb063 achieve good performance, the segmentation for image mdb058 deviates from the ground truth. Figures 10 and 11 are the segmentation results of Asymmetrical (ASYM) mdb104 and mdb111. Despite the non-convex boundaries and the lack of significant difference between the central region and the outer region in ASYM, the segmentation results are good. Architectural Distortion (ARCH) mdb165 and mdb117, the edges of architecturally distorted lesions are typically irregular and blend into the surrounding tissue, which can be challenging to discern. Although Figures 12 and 13 show the segmentation results, these outcomes seem limited in scope and likely generate false positives. Figures 14 and 15 show well-segmented results for Spiculated (SPIC) masses, mdb198 and mdb184, which are characterized by spiculated shapes resembling spikes emanating from a central point.

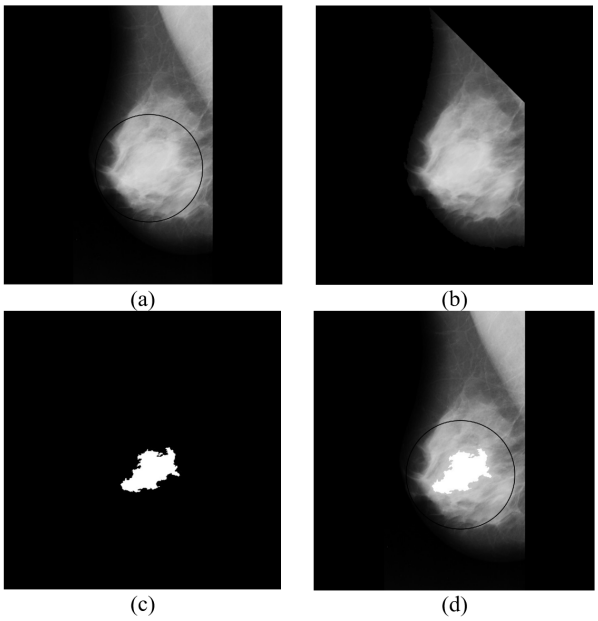

Figure 6. Result of CIRC lesion: a) Original mammogram mdb001 with ground truth (the lesion in the circle), b) Processed mammogram by the proposed method, c) Final segmented tumor mass by fast K-means method, d) Output image (black circle: ground truth, whiteshaded area: proposed method).

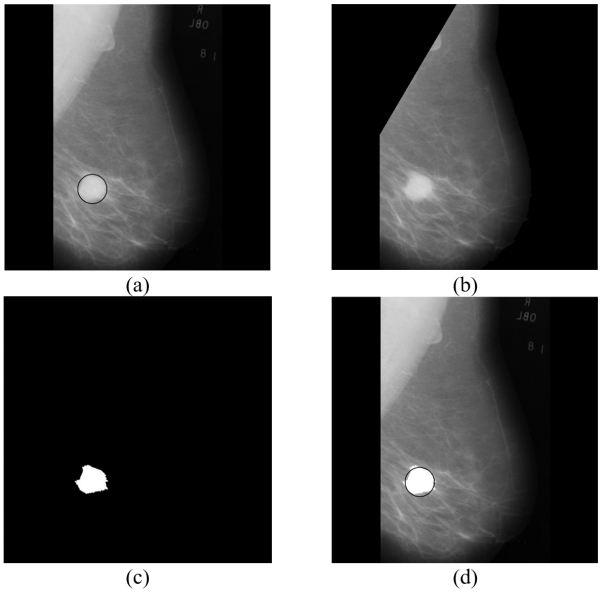

Figure 7. Result of CIRC lesion: a) Original mammogram mdb028, b) Processed mammogram, c) Final segmented tumor, d) Output image.

Despite the variations in tumor shapes, the fast k-means method effectively segments most tumors. The aforementioned results may be attributed to the selection of an suitable initial number of clusters and the enhancement of image efficiency.

Through the tumor extraction results of ten mammograms and the corresponding ground truth; the true positive (TP), true negative (TN), false positive (FP) and false negative (FN) are evaluated to determine performance

TABLE IV. The PSNR of four methods with different standard deviations Gaussian noise

Gaussian noise σ	VisuShrink	DnCNN	Benhassine [5]	Proposed Method
5	38.48	39.05	40.76	**42.49**
10	33.78	31.71	35.53	**37.06**
20	29.57	25.53	30.25	**31.16**
30	26.83	22.15	27.15	**27.75**

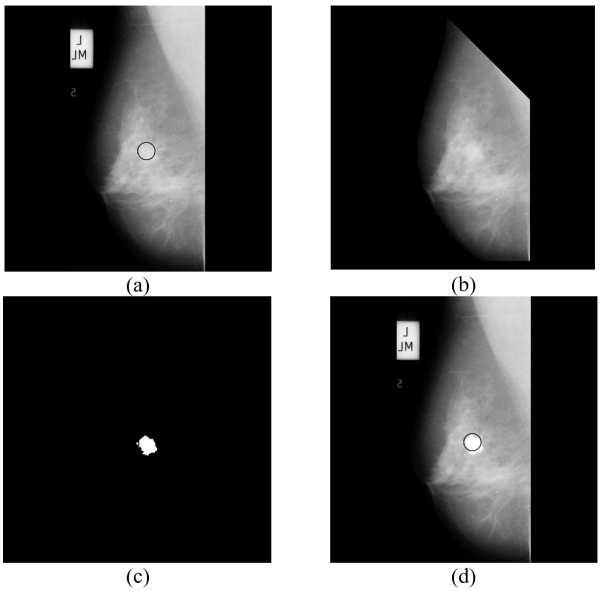

Figure 8. Result of MISC lesion: a) Original mammogram mdb063, b) Processed mammogram, c) Final segmented tumor, d) Output image.

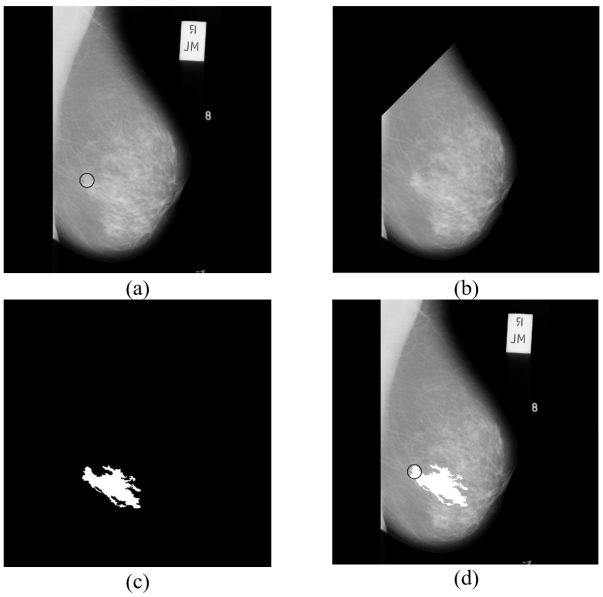

Figure 9. Result of MISC lesion: a) Original mammogram mdb058, b) Processed mammogram, c) Final segmented tumor, d) Output image.

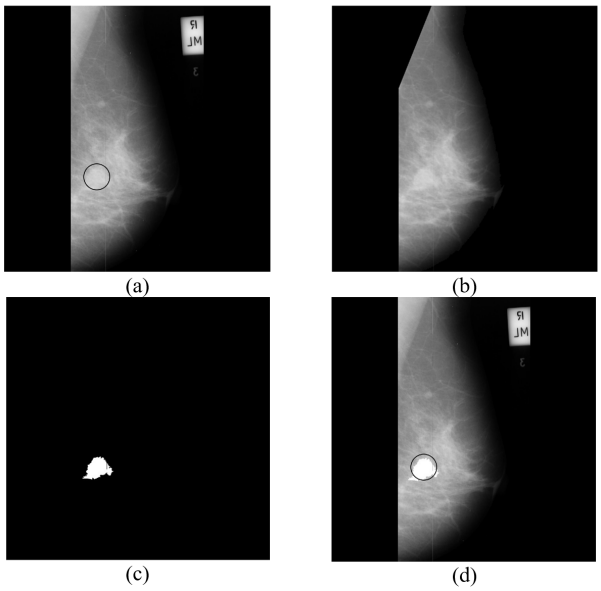

Figure 10. Result of ASYM lesion: a) Original mammogram mdb104, b) Processed mammogram, c) Final segmented tumor, d) Output image.

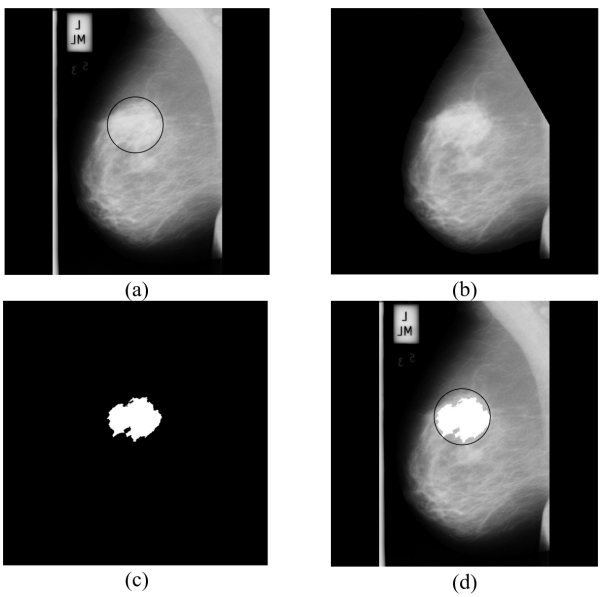

Figure 11. Result of ASYM lesion: a) Original mammogram mdb111, b) Processed mammogram, c) Final segmented tumor, d) Output image.

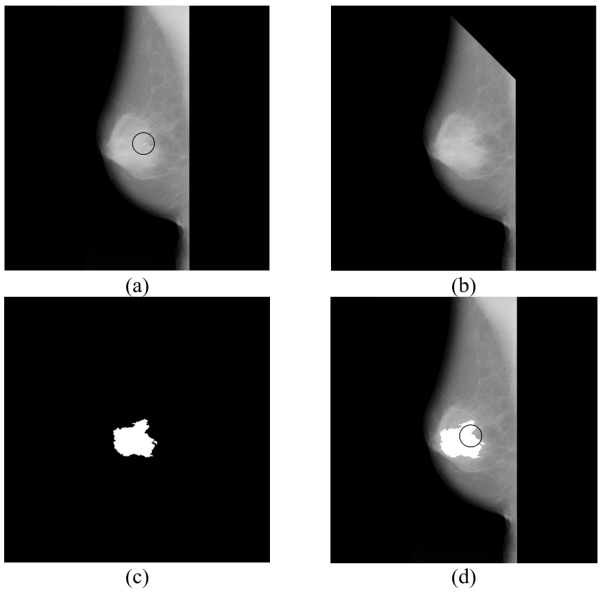

Figure 12. Result of ARCH lesion: a) Original mammogram mdb165, b) Processed mammogram, c) Final segmented tumor, d) Output image.

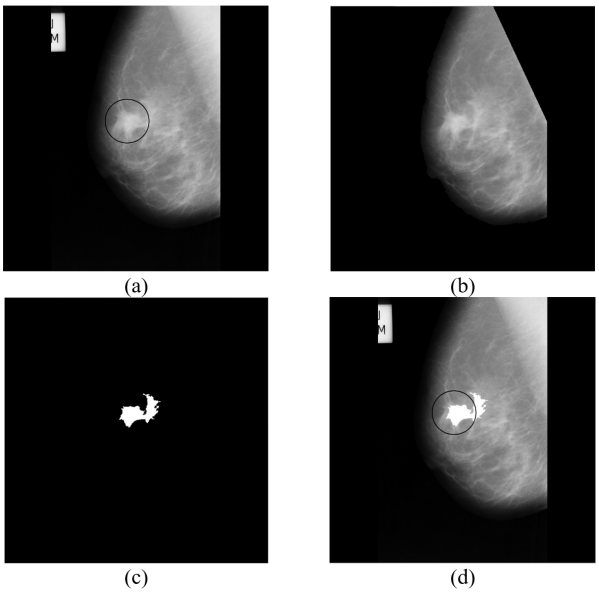

Figure 13. Result of ARCH lesion: a) Original mammogram mdb117, b) Processed mammogram, c) Final segmented tumor, d) Output image.

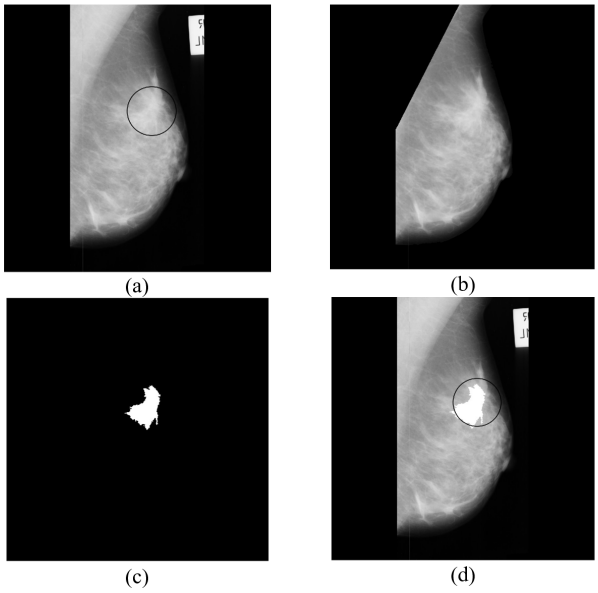

Figure 14. Result of SPIC lesion: a) Original mammogram mdb198, b) Processed mammogram, c) Final segmented tumor, d) Output image.

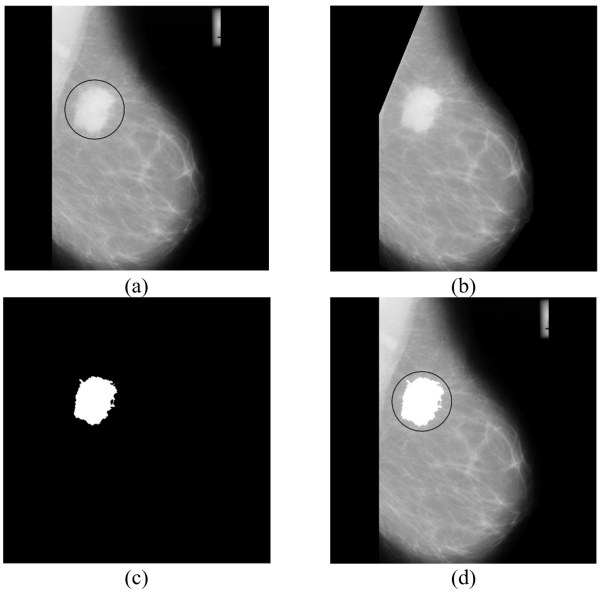

Figure 15. Result of SPIC lesion: a) Original mammogram mdb184, b) Processed mammogram, c) Final segmented tumor, d) Output image.

metrics such as:

$$Accuracy\ (Acc) = \frac{TP + TN}{TP + TN + FP + FN} \tag{20}$$

$$Sensitivity\ (Sen) = \frac{TP}{TP + FN} \tag{21}$$

$$Specificity\ (Spec) = \frac{TP}{TP + FP} \tag{22}$$

Table V shows the segmentation results, which demonstrate that the proposed approach attains an average accuracy of 98.15% and specificity of 99.56%. Because the ground truth is represented by a circle that can extend beyond the tumor mass, the FN is relatively high, resulting in a low sensitivity of only 62.81%.

Table VI presents the segmentation results of other authors, demonstrating that the segmentation results in this paper are comparable to those of others. However, when a larger number of images are used, the results may differ.

D. Classification results

Data were extracted from the mini-MIAS dataset, from which 50 benign and 50 malignant tumor images were selected to calculate six statistical features: the mean absolute value, the standard deviation, the skewness, the kurtosis, the RMS power, and the ratio the mean absolute values of two consecutive subbands of the approximation

TABLE V. The results of evaluation metrics in ten experimental mammograms

Images	Acc (%)	Sen (%)	Spec (%)
mdb001	90.79	34.61	100.00
mdb028	99.86	93.22	99.86
mdb063	99.82	76.84	99.84
mdb058	97.56	2.15	97.74
mdb104	99.77	84.85	99.87
mdb111	99.16	86.11	100.00
mdb165	98.71	42.97	98.74
mdb117	98.51	58.56	99.57
mdb198	98.83	71.93	99.94
mdb184	98.53	76.83	100.00
Average	98.15	62.81	99.56

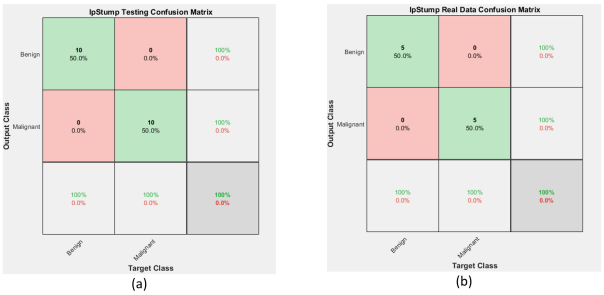

Figure 16. Confusion matrices, a) Test Data, b) Real Data

and detail coefficients of the SWT, from level 1 to level 8 using the 'db4' wavelet function. Therefore, each image is represented by 95 features recorded in a SWT feature matrix of size 100x96. Columns 1 to 95 represent the features, and column 96 represents the label of the image. The matrix is split into training (80%) and testing (20%) sets , which are used to build a classification model.

The small sample size is due to the limitations of the MIAS dataset, which only contains 52 images of malignant breast cancer. Five of these images were already used during tumor segmentation, leaving only 47. To reach the desired sample size of 50, additional images containing microcalcifications were included. While there are more benign images available, only 50 were selected to maintain data balance. These images were enhanced using our proposed approach and then used for feature extraction. These features are used to build a classification model based on boosting ensemble learning. The boosting ensemble method utilizes the fitcemsemble function from Matlab. It employs the LPBoost method with a decision tree as the base learner, a number of learning cycles set to 500, and no requirement for specifying the number of members. The results demonstrate the model's strong performance, achieving 100% accuracy on the training data. When applied to testing data and real data (ten mammograms listed in Table V, which are independent of the training data), the accuracy remains 100% for both datasets.

Figure 16 presents the confusion matrices for the test data and real data. The results showed that the model performed well and was stable. Despite the limited number of instances in the dataset, the features range from wide to narrow frequency bands of the frequency spectrum of the original image, which adequately capture the characteristics for classification. Additionally, the selection of a classifier suitable for these features enhances the model's performance in classification tasks.

The results were compared with those of the studies other authors [35], [36], [37] as listed in Table VII. This demonstrates that the boosting ensemble model outperforms the other methods.

5. Conclusion

Mammography stands at the forefront of early breast cancer detection and the comprehensive analysis of breast tumors. The method under consideration seeks to assist radiologists in image interpretation, thereby enhancing the collective effort against this pervasive ailment. Through the amalgamation of computational methodologies, breast cancer screening endeavors to attain heightened precision and mitigate instances of false positives, thus advancing the efficacy and reliability of diagnostic procedures in the ongoing battle against this formidable disease.

The proposed method substantiates its efficacy through three pivotal stages of medical analysis: image enhancement, segmentation, and classification. This progression notably enhances disease diagnosis accuracy, as evidenced by the ensuing experimental findings:

(a) Shift invariance is crucial in image denoising. The absence of shift invariance implies that minor adjustments in the input signal lead to significant fluctuations in the energy distribution between the transform coefficients at different scales and are therefore not suitable for denoising. Then, SWT-based denoising method with bivariate shrinkage and hybrid median filter provides a robust solution for image denoising.

(b) The vignette effect, when used with modified morphological operations, can increase the focus on details in the central area, thereby significantly increasing the contrast between objects and their surrounding area and thus improves segmentation. Noise reduction and contrast enhancement are computed separately and then fused using wavelet-based image fusion to select the dominant features for image enhancement.

(c) The choice of clustering fast K-means algorithms by automaticcally binning the histogram distribution makes this method more advantageous in the segmentation process.

(d) Feature extractions from the wavelet coefficients of SWT from level 1 to level 8 show that the features extracted at different scales correspond to the characteristics of the image in frequency ranges from wide to narrow. This ensures that feature extractions are sufficient for effective classification even when there are not many instances.

This study presents an analysis of noise reduction techniques for image enhancement and the extraction of statistical features for classification, utilizing the coefficients generated by SWT. Specifically, the segmentation process incorporates the K-means algorithm, highlighting its efficacy in partitioning images. Consequently, segmentation via SWT, coupled with the extraction of diverse features beyond statistical metrics for classification, emerges as a prospective avenue for future research endeavors. The integration of SWT coefficients offers a promising foundation for enhancing image quality through noise reduction,

TABLE VI. The segmentation results of other authors

No.	Authors	Methods	Number of images	Accuracy (%)
1	Shrivastava et al. (2017) [32]	Dispersed region growing algorithm	322	91.3
2	Soul et al. (2020) [33]	The electromagnetism-like algorithm	56	78.57
3	Wisaeng (2022) [10]	K–Means++ with Cuckoo Search	123	96.92
4	Ion et al. (2023) [34]	Fuzzy cellular automaton	118	98.66
5	Proposed approach	Fast and adaptive K-means	10	98.15

TABLE VII. Comparison of Classification Results with Different Methods on MIAS Dataset

No.	Authors	Classifier	Data size	Accuracy (%)
1	H. Pezeshki et al. (2019) [35]	SVM	58	91.37
2	V.S. Gnanasekaran et al. (2020) [36]	CNN	322	92.54
3	Jia Li et al (2023) [37]	Self-Attention Random Forest	322	98.79
4	Our result	LPBoosting Ensemble learning	100	100

while the utilization of advanced segmentation algorithms like K-means underscores the potential for more precise delineation of image regions. Moreover, the exploration of additional feature extraction methods beyond statistical measures promises to enrich the classification process, potentially yielding more robust and accurate results in diverse imaging applications.

Despite the advantages mentioned above, the wavelet transform-based denoising method, although it considers the relationship between components at different scales and achieves good results, does not yet respond to current development trends. Additionally, the data used is from a public database and has not been collected from hospitals. These two limitations will be addressed in future work.

Acknowledgment

This research is funded by Vietnam National University, Ho Chi Minh City (VNU-HCM) under grant number C2022-18-08.

References

[1] H. Sung *et al.*, "Globalcancer statistics 2020: Globocan estimates of incidence and mortality worldwide for 36 cancers in 185 countries," *CA: A Cancer Journal for Clinicians*, vol. 71(3), pp. 209–249, 2020.

[2] L. Sendur and I. W. Selesnick, "Bivariate shrinkage functions for wavelet-based denoising exploiting interscale dependency," *IEEE Transactions on Signal Processing*, vol. 50(11), pp. 2744–2756, 2002.

[3] S. Yin, H. Li, and et al, "Anisotropic bivariate shrinkage function for wavelet-based image denoising. signal processing," *Signal Processing*, vol. 91(8), pp. 2078–2090, 2011.

[4] W. Fan and W. Xiao, "Image denoising based on wavelet thresholding and wiener filtering in the wavelet domain," *The Journal of Engineering*, vol. 2019(19), pp. 6012–6015, 2019.

[5] N. E. Benhassine, A. Boukaache, and D. Boudjehem, "Threshold selection for wavelet-based denoising of medical images: a review," *International Journal of Biomedical Engineering and Technology*, vol. 36(2), pp. 94–109, 2021.

[6] K. Coffey and M. Jochelson, "Contrast-enhanced mammography for breast cancer screening and diagnosis," *European Journal of Radiology*, vol. 149, 2022. [Online]. Available: https://doi.org/10.1016/j.ejrad.2022.108228

[7] C. Tian *et al.*, *Multi-stage image denoising with the wavelet transform*, Pattern Recognition, 134, 109050, 2023.

[8] C. Liu and L. Zhang, "A novel denoising algorithm based on wavelet and non-local moment mean filtering," *Electronics*, vol. 12(14), p. 1461, 2019. [Online]. Available: https://journals.sagepub.com/doi/abs/10.1177/14680874221108588

[9] J. Wu and C. Hicks, "Breast cancer type classification using machine learning," *J. Pers. Med*, vol. 11(2), p. 61, 2021.

[10] K. Wisaeng, "Breast cancer detection in mammogram images using k-means++ clustering based on cuckoo search optimization," *Diagnostics*, vol. 12(12), p. 3088, 2022.

[11] N. F. Razali, I. S. Isa, S. N. Sulaiman, N. K. Abdul Karim, M. K. Osman, and Z. H. Che Soh, "Enhancement technique based on the breast density level for mammogram for computer-aided diagnosis," *Bioengineering*, vol. 10(2), p. 153, 2023.

[12] M. Talbi and R. Baazaoui, "Perspective chapter: New image denoising approach based on swt and 2-d dual-tree discrete wavelet transform," *IntechOpen*, 2023.

[13] M. Holschneider, R. Kronland-Martinet, J. Morlet, and P. Tchamitchian, "A real-time algorithm for signal analysis with the help of the wavelet transform," in *Wavelets: Time-frequency methods and phase space*, J. M. Combes and A. Grossmann, Eds. Springer-Verlag, 1989, pp. 289–297.

[14] G. P. Nason and B. W. Silverman, "The stationary wavelet transform and some statistical applications," *In Physica D: Nonlinear Phenomena*, vol. 88(3–4), pp. 181–200, 1995.

[15] S. Jean-Luc, F. Jalal, and M. Fionn, "The undecimated wavelet decomposition and its reconstruction," *IEEE Transactions on Image Processing*, vol. 16(2), 2007.

[16] G. Chen, W.-P. Zhu, and W. Xie, "Wavelet-based image denoising using three scales of dependency," *IET Image Processing*, vol. 6(6), pp. 756–760, 2012.

[17] R. Anitha and C. Chandrasekar, "A dual stage adaptive thresholding (DuSAT) for automatic mass detection in mammograms," *Computer methods and programs in biomedicine*, vol. 138, pp. 93–104, 2017.

[18] J. A. Hartigan, "A k-means clustering algorithm," *Journal of the Royal Statistical Society, Series C (Applied Statistics)*, vol. 28(2), pp. 100–104, 1979.

[19] D. Arthur, S. Vassilvitskii, and S. Blaine, "The k-means algorithm: A comprehensive survey and performance evaluation," *Electronics*, vol. 9(8), p. 1295, 2007.

[20] J. B. MacQueen, "A technique for efficiently grouping data clusters," in *Proceedings of the Berkeley Symposium on Mathematical Statistics and Probability*, vol. 1, 1967, pp. 281–297.

[21] R. Salman, V. Kecman, and Y. Li, "Two-stage clustering with k-means algorithm," *Engineering in Agriculture, Environment and Food*, vol. 11(3), pp. 110–125, 2018.

[22] *Change Filter Strength Radially Outward*, MATLAB documentation, MathWorks.

[23] A. Dixit, *Fast kmeans Algorithm Code*, Matlab Central File Exchange, MathWorks, 2023. [Online]. Available: https://au.mathworks.com/matlabcentral/fileexchange/44598-fast-kmeans-algorithm-code

[24] B. Esmaeil, A. Arnaout, and et al, "A statistical feature-based approach for operations recognition in drilling time series," *8th International Conference on Intelligent Computing, ICIC 2012*, vol. 7389, pp. 460–466, 2012.

[25] [Online]. Available: https://www.shiksha.com/online-courses/articles/ensemble-learning-boosting/

[26] Z.-H. Zhou, *Ensemble Methods: Foundations and Algorithms*. Chapman & Hall/CRC Press, 2012, ch. 2.

[27] J. Rocca. (2019) Ensemble methods: bagging, boosting and stacking. [Online]. Available: https//towardsdatascience.com/ensemble-methods-bagging-boosting-and-stacking-c9214a10a205

[28] M. Warmuth, J. Liao, and G. Ratsch, "Totally corrective boosting algorithms that maximize the margin," in *Proc. 23rd Int'l. Conf. on Machine Learning, ACM*, New York, 2006, pp. 1001–1008.

[29] M. I. A. Society, "Mini mammography database. retrieved from http://www.wiau.man.ac.uk/ services/miasimia-smini.htm," 2008.

[30] S. Verma and P. K. Mishra, "A comparative analysis of image compression by different wavelets techniques using matlab," *International Journal of Research in Engineering and Applied Sciences*, 2017.

[31] Y. T. H. Hua, G. H. Nguyen, and L. V. Dang, "Detection of abnormalities in mammograms by thresholding based on wavelet transform and morphological operation," in *Intelligent Systems and Networks (ICISN 2023), Lecture Notes in Networks and Systems*, vol. 752. Springer, 2023, pp. 496–506.

[32] A. Shrivastava, A. Chaudhary, D. Kulshreshtha, V. P. Singh, and R. Srivastava, "Automated digital mammogram segmentation using dispersed region growing and sliding window algorithm," in *2nd International Conference on Image, Vision and Computing*, 2017.

[33] K. B. Soulami, M. N. Saidi, B. Honnit, C. Anibou, and A. Tamtaoui, "Detection of breast abnormalities in digital mammograms using the electromagnetism-like algorithm," *Multimed Tools Appl*, 2020. [Online]. Available: https://doi.org/10.1007/s11042-018-5934-4

[34] I.-A. Ion, C. Moroz-Dubenco, and A. Andreica, "Breast cancer images segmentation using fuzzy cellular automaton," *Procedia Computer Science*, vol. 225, pp. 999–1008, 2023.

[35] H. Pezeshki, M. Rastgarpour, A. Sharifi, and S. Yazdani, "Extraction of spiculated parts of mammogram tumors to improve accuracy of classification," *Multimed Tools Appl*, 2019. [Online]. Available: https://doi.org/10.1007/s11042-019-7185-4

[36] V. S. Gnanasekaran, S. Joypaul, P. M. Sundaram, and D. D. Chairman, "Deep learning algorithm for breast masses classification in mammograms iet image processing," *IET Image Processing*, vol. 14(12), pp. 2860–2868, 2020.

[37] J. Li, J. Shi, J. Chen, Z. Du, and L. Huang, "Self-attention random forest for breast cancer image classification," *Frontiers in Oncology*, 2023.

Yen Thi Hoang Hua received her M.Sc. degree of Physics in 2007 and currently enrolled in a doctoral program of Engineering Physics from the University of Science-Vietnam National University, Ho Chi Minh City. She is a Lecturer at Department of Physics and Computer Science, Faculty of Physics and Engineering Physics, University of Science-VNU HCM, Vietnam. Her area of interest includes Signal and Image Processing, Machine Learning, Deep Learning. Her email is hthyen@hcmus.edu.vn

Giang Hong Nguyen received the M.Sc. degree in Radio Physics and Electronics (Speciality of appied physics) from the University of Science,Vietnam National University, Ho Chi Minh City, Vietnam in 2021. He is currently PhD student of Engineering Physics fromUniversity of Science, VNU HCM, Vietnam. His area of research interests are Signal and Image Processing, Machine Learning.

LUONG Bao Binh earned his Ph.D. in Geodesy in 2011 from Graz University of Technology, Austria. Currently, he serves as the Chair of the Geomatics Engineering Department at Ho Chi Minh City University of Technology. His research focuses on geodesy and geoid computation, as well as LiDAR and image processing for UAV and mobile mapping systems.

Dang Van Liet received his Ph.D. in Mathematics – Physics from the University of Ho Chi Minh City (now Vietnam National University, Ho Chi Minh City) in 1995. He is an invited Associate Professor at the Dept. Physics – Computer Science at the University of Science (Vietnam National University, Ho Chi Minh City). His areas of interest are Signal and Image Processing, Machine Learning, Gravity and Magnetic data analysis. His email is dangvanliet@gmail.com